ISSN 1001-0742
CN 11-2629/X

2012

Volume 24
Number 4

JOURNAL OF ENVIRONMENTAL SCIENCES

ELSEVIER
Science Press

Sponsored by
Research Center for Eco-Environmental Sciences
Chinese Academy of Sciences

ISSN 1001–0742 **Journal of Environmental Sciences** Vol. 24 No. 4 2012

CONTENTS

Serial parameter: CN 11-2629/X*1989*m*210*en*P*27*2012-4

Available online at www.sciencedirect.com
ScienceDirect
Journal of Environmental Sciences 2012, 24(4) 757–764
JOURNAL OF ENVIRONMENTAL SCIENCES
ISSN 1001-0742
CN 11-2629/X
www.jesc.ac.cn

Preparation of $Fe_xCe_{1-x}O_y$ solid solution and its application in Pd-only three-way catalysts

Jianqiang Wang[1,2], Meiqing Shen[1,3,*], Jun Wang[1], Mingshan Cui[1], Jidong Gao[2], Jie Ma [2], Shuangxi Liu[2]

1. Key Laboratory for Green Chemical Technology of State Education Ministry, School of Chemical Engineering & Technology, Tianjin University, Tianjin 300072, China. E-mail: jianqiangwang@tju. edu.cn
2. China Automotive Technology & Research Center, Tianjin 300162, China
3. State Key Laboratory of Engines, Tianjin University, Tianjin 300072, China

Received 22 April 2011; revised 19 July 2011; accepted 10 August 2011

Abstract

FeO_x-CeO_2 mixed oxides with increasing Fe/(Ce+Fe) atomic ratio (1–20 mol%) were prepared by sol-gel method and characterized by X-ray powder diffraction (XRD), Brunauer-Emmett-Teller (BET) and Hydrogen temperature-programmed reduction (H_2-TPR) techniques. The dynamic oxygen storage capacity (DOSC) was investigated by mass spectrometry with CO/O_2 transient pulses. The powder XRD data following Rietveld refinement revealed that the solubility limit of iron oxides in the CeO_2 was 5 mol% based on Fe/(Ce+Fe). The lattice parameters experienced a decrease followed by an increase due to the influence of the maximum solubility limit of iron oxides in the CeO_2. TPR analysis revealed that Fe introduction into ceria strongly modified the textual and structural properties, which influenced the oxygen handling properties. DOSC results revealed that Ce-based materials containing Fe oxides with multiple valences contribute to the majority of DOSC. The kinetic analysis indicated that the calculated apparent kinetic parameters obey the compensation effect. The three-way catalytic performance for Pd-only catalysts based on the Fe doping support exhibited the redundant iron species separated out of the CeO_2 and interacted with the ceria and Pd species on the surface, which seriously influenced the catalytic properties, especially after hydrothermal aging treatment.

Key words: FeO_x-CeO_2; solubility limit; dynamic oxygen storage/release capacity; three-way catalytic performance
DOI: 10.1016/S1001-0742(11)60816-4

Introduction

Environmental problems associated with air pollution are now deteriorating our entire earth and represent some of the most formidable challenges facing global society in the future. Furthermore, the rarity of noble metal catalysts presents serious hurdles to the implementation of clean energy technologies on a global scale. Environmental and economic considerations have led engineers and scientists to anticipate the need to develop a clean, renewable and sustainable technology As outstanding oxygen storage materials (OSMs), ceria-based materials have been widely used in the three-way catalysts (TWCs). The reason for extensive use of ceria as an active ingredient in the TWCs is emerge from its reversible oxygen storage and release capacity (OSC) in response to fluctuating oxygen concentration, ensuring the targeted air/fuel ratios and emission control (Trovarelli, 1996). This unique property of ceria has been triggered off many salient applications of industrial significance.

Although ceria has been studied extensively, under elevated conditions ceria becomes inefficient with time and many innate properties will be affected. Hence, much effort has been made to synthesize ceria-based mixed oxides for better thermal durability and improved OSC performance. Modification of ceria is a key issue in the development of efficient catalyst formulations for treatment of auto exhaust processes and other applications. The doped ceria enhances the surface area and can sustain toward sintering during the high temperature long-term anneal due to the cooperative nature of the cations of the mixed oxides (Shen et al., 2009; Wang et al., 2011). Further, the combination of different cations in the oxide matrix can produce materials with novel structural and electronic properties which may lead to high catalytic activity. The Fe doped ceria-based materials have been widely used in catalysis, adsorption and sensors (Bao et al., 2008; Li et al., 2001; Pérez-Alonso et al., 2005; Liang et al., 2009; Wang et al., 2011).

Substitution of transition metal like Fe in CeO_2 fluorite structure shows superior catalytic activity and brings down the cost of the catalyst considerably. However, aliovalent ions doped samples are thermally less stable and prone to phase segregation. According to Noronha et al. (2003), precious metal particles were covered by aggregated tran-

* Corresponding author. E-mail: mqshen@tju.edu.cn

sition metal species after redox ageing, and this is going to decrease the catalytic activity severely. In order to make good utilization of transition metal but not to poison the precious metals, it is very necessary that the base metal ions be fixed and retain immobile, especially after thermal treatment. The improvement of the catalytic activity and resistance to high temperature of these alternative systems would be desirable to use them as co-catalysts and, therefore, reduce the amount of expensive precious metals in conventional catalytic devices. Further, it is desirable to determine the effect of dopants on the lattice parameters and their solubility limits in the cubic fluorite structure phase.

The present contribution focuses on the $Fe_xCe_{1-x}O_y$ solubility limits by XRD Rietveld refinement analysis. The oxygen storage/release capacity of $Fe_xCe_{1-x}O_y$ samples was investigated. The relationship between solid solution and its activity for dynamic OSC (DOSC) and the three-way catalytic (TWC) performance was proposed.

1 Experimental

1.1 Sample preparation

Fe doping ceria mixed oxides ($Fe_xCe_{1-x}O_y$, x = 0.01, 0.03, 0.05, 0.07, 0.1, 0.15, 0.2) were synthesized by citric acid sol-gel method. The nitrates of Ce (Zibo Rongruida, China), and Fe (Tianjin Guangfu, China) were used as starting materials. Citric acid was added as complex agent, and glycol was used as additive. After continuous stirring for 2 hr, the mixed solution was treated at the temperature of 80°C overnight to form the sponge yellow gel. Then, the gel was dried at 100°C for 3 hr and milled before calcination. The dried gel was calcined at 300°C for 30 min and then at 500°C for 5 hr. The CeO_2 prepared with the same method were reference samples.

The Pd loading was achieved by impregnating $Fe_{0.05}Ce_{0.95}O_y$ and $Fe_{0.1}Ce_{0.9}O_y$ with $Pd(NO_3)_2$ aqueous solutions with 0.5 wt.% Pd loading. The solid products were separated, dried at 100°C for 2 hr, and then calcined at 500°C for 3 hr. These as-prepared samples were called fresh samples, and were designated as $Pd/Fe_{0.05}Ce_{0.95}O_y$ and $Pd/Fe_{0.1}Ce_{0.9}O_y$. Aged samples were obtained by hydrothermally aging the as-prepared catalysts at 1050°C or 10 hr in a 10% steam-air condition, which were designated as $Pd/Fe_{0.05}Ce_{0.95}O_y$a and $Pd/Fe_{0.1}Ce_{0.9}O_y$a respectively.

1.2 Characterization

The structure of the mixed oxides was identified by X-ray diffraction (XRD) on an X'Pert Pro diffractometer (The Netherlands) using Fe-filtered Co $K\alpha$ radiation and a power of 45 kV × 30 mA. The intensity data were collected at 25°C over a 2θ range of 20°–90° with a 0.03° step size.

The X-ray diffraction analyses were carried out at room temperature on a Rigaku D/max 2500 v/pc diffractometer (Japan) with Cu-$K\alpha$ radiation a power of 40 kV × 2 mA. The intensities of the XRD patterns were obtained in the 2θ range between 20° and 90° with a step of 0.02° and a measuring time of 2.0 sec each point. The MAUD (material analysis using diffraction) software was applied to refine the crystalline structures of the solids with the Rietveld method.

H_2-TPR experiments were performed using a Micromeritics AutoChem 2910 (America). The catalyst was first purged under N_2 (30 mL/min) at 200°C for 1 hr and then cooled to room temperature. The sample was then exposed to a flow of 5% H_2/Ar (30 mL/min) while the temperature was ramped from room temperature to 900°C at a rate of 10°C /min.

1.3 Reaction test

Two types of OSC measurements were conducted, including dynamic CO-He pulses and transient CO-O_2 pulses (Wang et al., 2011). Concentrations of CO, O_2, CO_2, Ar, and He in the outlet gas were monitored on-line by Hiden HPR20 (England) quadrupole mass spectrometer. Twenty-five milligram sample diluted with 40 mg quartz sand was placed in the heat transfer reactor (10 mm diameter) at a height of 1.5 mm, with additional 4 mm redistributing layers of quartz wool on the two sides of catalysts bed. Flow rate of every pulse is 300 mL/min. Dead volume of the system was 3.5 mL. Errors induced by residence time and possible CO+O_2 turbulent mixing involved catalytic combustion can be limited to 2% during OSC quantifications. Before both of the testing modes, samples were pre-oxidized under O_2(2%)/Ar(1%)/He atmosphere, and then purged under He until no $^{32}O_2$ signal detected. The two experimental modes are described as the follows: (1) transient oxygen release measurements at 500°C were conducted under consecutive CO (5 sec)-He (40 sec) conditions. CO(4%)/Ar(1%)/He and He were alternately pulsed for 10 times in sequence. (2) dynamic CO-O_2 pulses (DOSC) measurements were operated from 200 to 500°C with the interval of 100°C. At each testing temperature, O_2 (2%)/Ar(1%)/He and O_2(2%)/Ar(1%)/He were pulsed alternately in sequence at the frequency of 0.1 Hz. The simulated plug flows repeated for more than five cycles to guarantee the reproducibility of collected response curves.

The three-way catalytic activity experiment were tested in the fixed-bed reactor at a stoichiometric A/F ratio of λ = 1 with the simulated exhaust gas containing: CO 2%, NO 0.1%, C_3H_8 0.1%, CO_2 12%, O_2 1.5% and N_2 (balance). The space velocity was 50,000 hr^{-1}. Four hundred milligrams of a catalyst diluted by quartz sand to 1.8 mL was placed at the bottom of quartz reactor. A standard test consisted of increasing the temperature from room temperature to 700°C at 10°C/min. Concentrations of CO, CO_2, NO, and C_3H_8 were quantified by an IR detector (America).

2 Results and discussion

2.1 Characterization

2.1.1 XRD analysis

Figure 1 illustrates the powder XRD patterns of the as prepared samples of $Fe_xCe_{1-x}O_y$ at different dopant

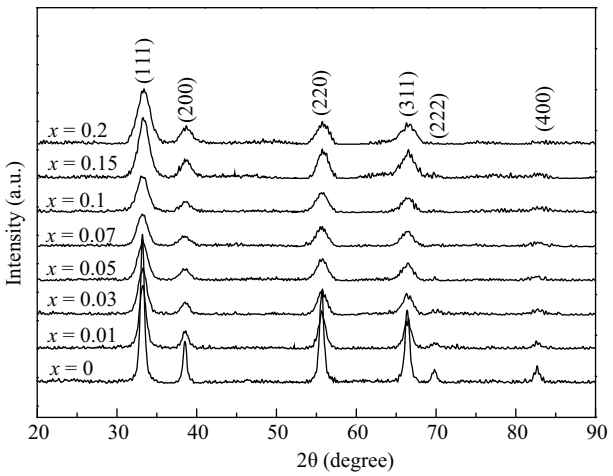

Fig. 1 XRD pattern of $Fe_xCe_{1-x}O_y$.

contents. The diffraction peaks were indexed to (111), (200), (220), (311), (222) and (400) planes, matching well those of the face-centered cubic fluorite structure of CeO_2 (JCPDS No. 43-1002). It can be seen that no FeO_x phases (FeO or Fe_2O_3) can be identified for all samples. This demonstrates that iron oxide exists as highly dispersed or amorphous surface species or the iron amount is low. From Fig. 1, it is seen that all diffraction peaks were broadened, which indicated the fine nature of the small particles, in agreement with previous results (Xue et al., 2007).

The lattice parameters of the as-prepared $Fe_xCe_{1-x}O_y$ samples were calculated by Rietveld refinement analysis. The Rietveld's method has given a reasonable fit of the diffraction profiles (R_{wp} < 12%). Rietveld refinement analysis indicated that the XRD pattern could be indexed satisfactorily to the fluorite structure with a space group Fm3m. The values of the lattice parameters and oxygen ion vacancies for all the samples are listed in Table 1. Oxygen ion vacancies increased with Fe content (Fig. 2) indicating that Fe ions are possibly substituted for Ce^{4+} in the fluorite lattice. A similar observation was also noted by Murugan et al. (2005) and Bera et al. (2002) for their Mn/CeO_2 and Cu/CeO_2 samples. The relationship between the lattice parameter and the content of dopant iron is shown in Fig. 3. With increasing Fe content, the lattice parameter for the fluorite solid solutions decreases linearly up to 5.3978(13) Å for x < 0.05, confirming that some Fe^{n+} ions are incorporated in the ceria lattice forming homogeneous $Fe_xCe_{1-x}O_y$ solid solutions (x: 0.01–0.05). It is reasonable that iron ions have been incorporated into the CeO_2 lattice to form solid solutions by considering the radius of Fe ions (r^{2+}_{Fe} = 0.074 nm; r^{3+}_{Fe} = 0.064 nm) is smaller than that of Ce^{4+} (0.101 nm). It is noteworthy that the lattice parameter for $Fe_{0.07}Ce_{0.93}O_y$ is significantly increased, suggesting that the iron ions segregate gradually from $Fe_xCe_{1-x}O_y$ solid solutions with further increase of Fe content. So we can conclude that the solution limit of FeO_x in ceria is 5%.

2.2 H_2-TPR

H_2-TPR profiles of Fe doped samples ($Fe_{0.05}Ce_{0.95}O_y$ and $Fe_{0.1}Ce_{0.9}O_y$) and reference samples (CeO_2) are presented in Fig. 4. The H_2-TPR results demonstrate that Fe doping improved the oxygen buffering capability, which considered the key for the superior DOSC performance. For Fe_2O_3, there are two reduction peaks centered at 430 and 726°C, corresponding to the reduction of Fe_2O_3 to Fe_3O_4 and of FeO to partial Fe^0, respectively (Liu and He, 2010; Liu et al., 2010). For CeO_2, the H_2 consumption peaks are observed at 511 and 801°C, respectively, which are attributed to the release of the surface oxygen and the bulk oxygen of ceria (Fan et al., 2008). Synergistic interaction between Ce and Fe in the mixed solid solution gives rise to low temperature reduction. The H_2-TPR analysis reveals that the reduction peaks shift to lower temperatures when Fe is doped. As illustrated in Fig. 5, three reduction peaks at 428°C (peak α), 683°C (peak β) and 817°C (peak γ) can be observed for $Fe_{0.05}Ce_{0.95}O_y$ sample, and the peaks are 382, 642 and 801°C for $Fe_{0.1}Ce_{0.9}O_y$ sample. The α and β peaks can be ascribed to the step-wise reduction of iron oxide and the reduction of surface/subsurface oxygen species of ceria (Zhang et al., 2010). When Fe is incorporated into the CeO_2 lattice to substitute Ce^{4+} cations, a solid solution can formed. The charge unbalance and lattice distortion take place within the structure of CeO_2, and thus lead to the generation of oxygen vacancies, which can bond less stable oxygen species. These weaker (active) adsorbates are reduced by H_2 at lower temperatures. It suggests that there is a certain synergistic interaction between Fe–O and Ce–O. The oxygen species being able to be reduced in such a range of temperatures are believed to make major contributions to DOSC and DOSR performances. The mutual promotion effect of ceria and Fe species is believed to be essential for the higher DOSC and DOCR of the Fe-doped samples. The γ peak represents the release of the bulk oxygen of ceria.

To derive the effect of substituting transition metal ions in ceria lattice on its oxygen storage/release property, the total oxygen storage capacity (TOSC) was estimated by the integrated amount of H_2 consumed during the H_2-TPR test. The results are listed in Table 2 along with ceria consumed 0.88 mmol/g. TOSC is related to the contents and the reducibility of the ceria components in certain materials. Although the ceria content is lowered in the Fe doped samples, the TOSC was improved due to the contribution of Fe dopants and its synergistic effect with Ce. It noteworthy that the amount of oxygen released at

Table 1 Texture characterizations for $Fe_xCe_{1-x}O_y$ samples

Sample	BET (m^2/g)	Lattice parameter (Å)	Oxygen vacancy (%)	R_{wp} (%)	Theoretic lattice parameter (Å)
$Fe_{0.01}Ce_{0.99}O_y$	33.7	5.4092 (10)	5.6	10.65	5.4104
$Fe_{0.03}Ce_{0.97}O_y$	49.0	5.4090 (11)	9.6	8.46	5.4052
$Fe_{0.05}Ce_{0.95}O_y$	42.3	5.3978 (13)	12.8	8.84	5.4000
$Fe_{0.07}Ce_{0.93}O_y$	34.4	5.4047 (18)	17.0	10.20	5.3948

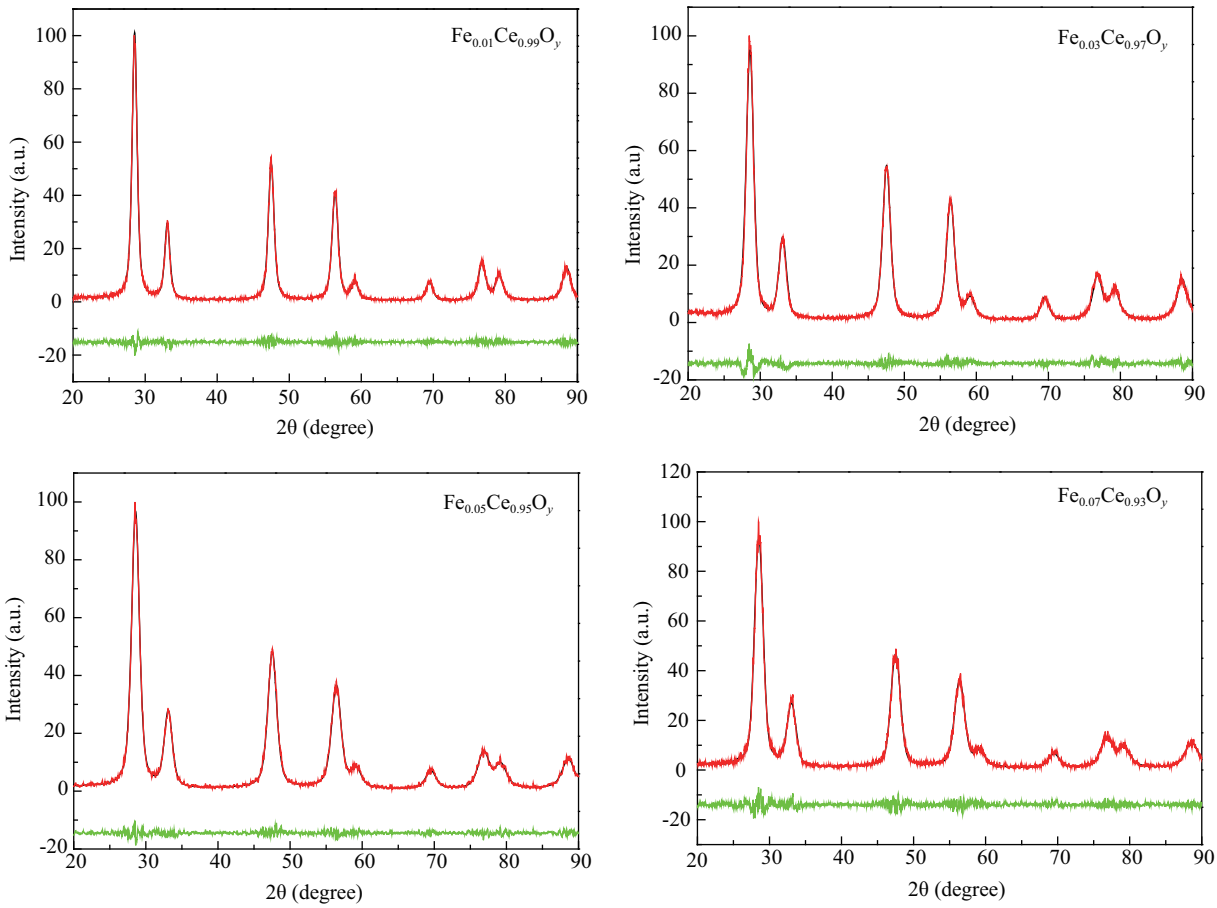

Fig. 2 Rietveld refinement plots of the $Fe_xCe_{1-x}O_y$.

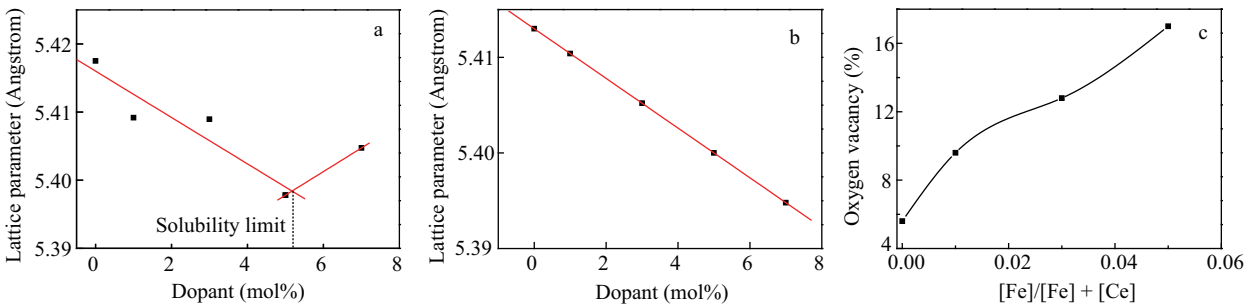

Fig. 3 Dependence of the lattice parameter with [Fe]/([Fe]+[Ce]). (a) lattice parameters based on XRD Rietveld refinement; (b) theoretic lattice parameters based on Vegard's law (Kim, 1989); (c) oxygen vacancy with [Fe]/([Fe]+[Ce]).

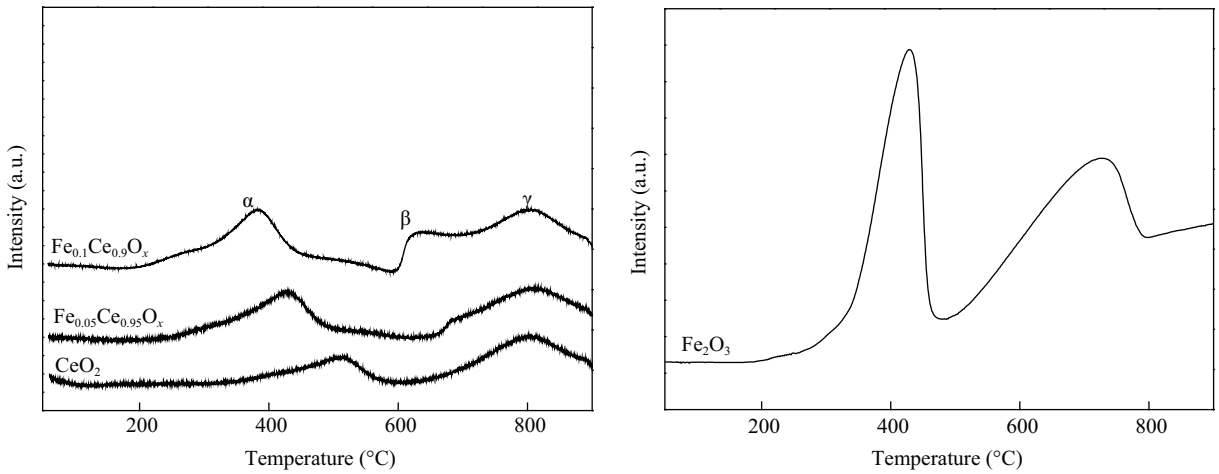

Fig. 4 H_2-TPR profiles of CeO_2, $Fe_{0.05}Ce_{0.95}O_y$, $Fe_{0.1}Ce_{0.9}O_y$ and Fe_2O_3 samples.

Table 2 Oxygen releasing amount in different temperature ranges by H_2-TPR

Sample	Content of oxygen releasing (mmol/g)		
	< 600°C	> 600°C	TOSC
$Fe_{0.05}Ce_{0.95}O_y$	0.59	0.65	1.24
$Fe_{0.1}Ce_{0.9}O_y$	0.71	0.82	1.53
CeO_2	0.27	0.61	0.88

low temperatures for samples by iron doping was much higher than that of CeO_2, indicating the favored oxygen releasing kinetics at low temperature for Fe doped samples.

2.3 Oxygen storage/release capacity

2.3.1 Total OSC with CO-He pulses

To study the total amount of lattice oxygen available under anaerobic atmosphere, CO pulses with He intervals were used to monitor the oxygen migration behavior of the catalysts. Figure 5 depicts the OSC data in transient CO-He pulses. TOSC is calculated by adding up the OSCs during the ten consecutive CO pulses. The TOSC are increased with increasing Fe doping amount.

Figure 5 shows that from the first to tenth CO pulse, OSC during each CO pulse does not linearly increase with the Fe doping amount. This would mean that redundant Fe doping would influence the oxygen handling properties. During initial CO pulses, CO oxidation occurs mostly by using the surface and near-surface oxygen of the catalysts. After the depletion of such a kind of oxygen species, the rest of the CO pulses are mostly oxidized by bulk oxygen in a two-step process, including the adsorption of CO on the catalyst' surface and its subsequent combination with bulk oxygen species. Bulk oxygen migration is the rate-determining step here, which can be considered as a function of the intrinsic structure of the material (Vidal et al., 2001). A direct relationship between lattice defects and OSC was discussed by Mamontov et al. (2000), and they suggest that oxygen defects are the sources of OSC in ceria-based material. Moreover, microstructure variation of ceria-based materials induced by doping with aliovalent oxides could improve lattice oxygen mobility (Fornasiero, et al., 1999). This is the primary reason that ceria-based oxide doping by aliovalent ions are being used in TWC as the improved generations of promoters or support oxides.

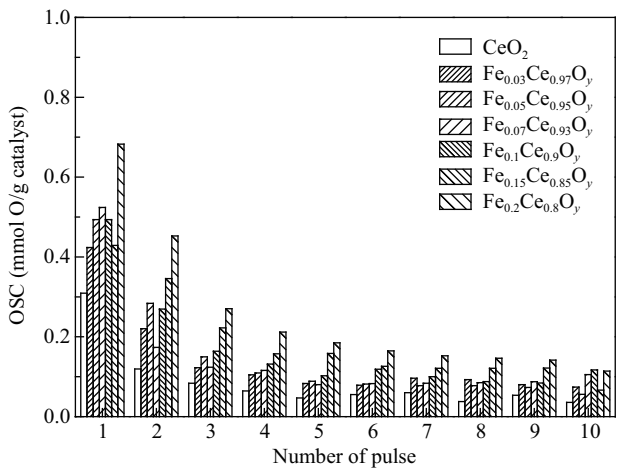

Fig. 5 OSC performance of different samples with alternate pulses of CO(4%)/Ar(1%)/He and pure He at 500°C.

In the CeO_2 fluorite structure, cations are in eightfold coordination with their nearest neighbors and each anion is surrounded tetrahedrally by four cations. The $Fe_xCe_{1-x}O_y$ solid solution of the fluorite-type oxides is obtained by the substitution of Fe cations for Ce cations. Doping the fluorite oxide with aliovalent cations, whose valency is smaller than that of the host cation, creates oxygen vacancies to achieve electronically neutrality in the substituted fluorite lattice. The presence of oxygen vacancy is the key factor for bulk oxygen mobility. The structural distortion induced by dopant ions substitution result in enhanced DOSC performance compared to pure ceria.

2.3.2 Dynamic OSC with CO and O_2 pulses

The DOSC measurement simulates the oscillations of exhaust composition between lean and rich conditions, and evaluates the oxygen storage/release capability of the catalytic materials in setting off the frequent lean-rich oscillations. CO oxidation and O_2 consumption are taken as the model reactions under rich and lean conditions respectively and the results are shown in Fig. 6. It is obvious that the DOSC of Fe doped samples are higher than those of corresponding CeO_2. It suggests that the oxygen vacancies and the lattice distortion are produced by Fe doped for charge compensation and radius effect, which is the essential reason for OSC promotion (Li et al., 2009). According to Lambrou and Efstathiou (2006), iron significantly favored the formation of superoxide (O_2^-) species on CeO_2 to weaken the bond strength of O_2^- with the ceria surface, which is involved in the oxygen transport and storage on CeO_2. Further, transition metal oxide can store/release oxygen under redox conditions, which are contributed to the superior OSC performance. In addition, Wang and Gorte (2003) suggested that the ion oxide may lower the barrier for oxygen transfer based on the different enthalpy change: going from CeO_2 to Ce_2O_3 760 kJ/mol of O_2, while 460 kJ/mol of O_2 for Fe_2O_3 to Fe_3O_4. So we can concluded that Fe doped may promote formation of Ce^{3+} ions due to the smaller size of iron cations that take part in removing the strain associated with the increase of ionic size accompanying the $Ce^{4+} \longrightarrow Ce^{3+}$ transition.

Generally, DOSC can be enhanced with increasing reaction temperatures, because higher amount of lattice oxygen becomes available for the reactions and the oxygen spillover processes have been accelerated (Zhao et al., 2007). The bulk oxygen migration capability is promoted by the introduction of Fe, as indicated by the improved DOSC performances of $Fe_xCe_{1-x}O_y$ samples especially at high temperatures. It is noted that the DOSC does not linearly increase with the Fe doping amount. This would mean that the increasing presence of Fe at the surface modifies the interaction with oxygen. Probably, this is related to the intrinsic arrangement of the dopant-vacancy pair, which would make bulk diffusion more difficult with respect to optimum Fe doping samples.

The dynamic oxygen storage rate (DOSR) defined as the amount of oxygen stored and released in the first

second of every oscillation cycle and acted as a method to characterize oxygen storage material performance (Hori et al., 1999). DOSR can be calculated as:

$$\text{DOSR} = \int_0^1 \text{CO}_2 \text{ signal} = \text{Rate}([\text{CO}_2/\text{sec}]) \quad (1)$$

where, $\int_0^1 \text{CO}_2$ signal is the integrated CO_2 peak area from 0 to 1 sec.

The results of DOSR over all samples are summarized in Table 3. It is obvious that the DOSR of samples containing Fe are superior to those of corresponding CeO_2. The presence of Fe ions near Ce^{4+} site coordinated with O^{2-} make the transformation of $Ce^{4+} \longrightarrow Ce^{3+}$ easier than ceria, since low valance iron cations will disturb the charge equilibrium and distortion in ceria lattice resulting in the oxygen vacancies formation associated with Ce^{3+} sites (Fernández-García et al., 2002). Energy between Ce^{4+}/Ce^{3+} couple is inferred to be altered by Fe disturbing. Role of oxygen vacancies and lattice distortion for DOSC promotion should not be excluded by Fe introducing. It should be noted that the DOSR are not linearly increased with the Fe doping content, in agreement with the DOSC results. It suggested that the surface Fe-enrichment is formed, when the iron dopants content are in excess of solubility limits, which can baffle the oxygen mobility.

To better understand the effect of Fe doping for specific reaction procedures, kinetic parameters were investigated. Figure 7 shows the relationship between the ln$k$ and $1/T$ (10^3). As the reaction rate constant of CO oxidation, k is calculated by dividing from DOSR. Fitting reaction rate data to the Arrhenius equation provides the pre-exponential factors (ln$A$) and activation energies (E_a). As

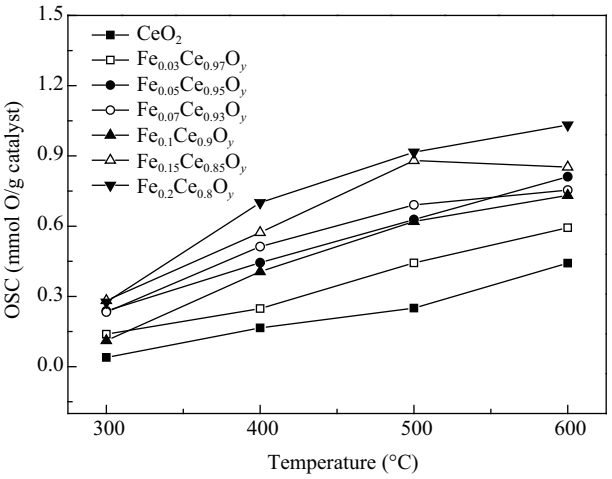

Fig. 6 Effect of Fe doping on the DOSC with alternate dynamic pulses of CO(4%)/Ar(1%)/He and O_2(2%)/Ar(1%)/He under 0.1 Hz.

Table 3 DOSR for $Fe_xCe_{1-x}O_y$ samples

Catalyst	DOSR (μmol O/(g_{cat}·sec))			
	300°C	400°C	500°C	600°C
$Fe_{0.05}Ce_{0.95}O_y$	9.0	12.9	16.9	23.7
$Fe_{0.1}Ce_{0.9}O_y$	6.2	17.0	19.2	29.4
$Fe_{0.15}Ce_{0.85}O_y$	17.4	20.8	33.4	38.3
$Fe_{0.2}Ce_{0.8}O_y$	9.3	10.4	16.4	24.3
CeO_2	0	8.8	12.0	27.4

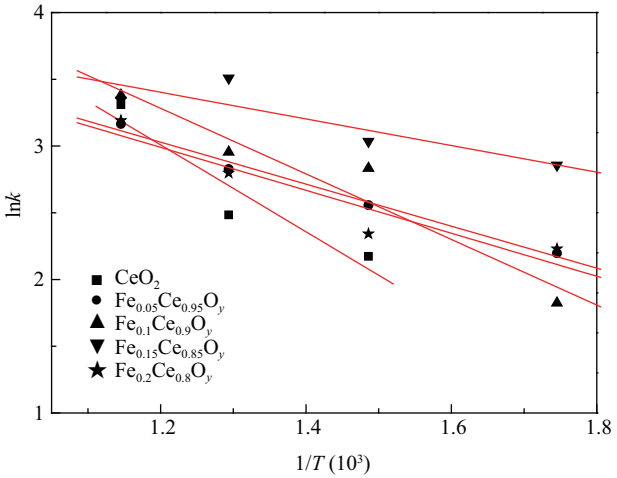

Fig. 7 Arrhenius plot of $Fe_xCe_{1-x}O_y$ samples.

Table 4 Pre-exponential factor and apparent activation energy calculated for $Fe_xCe_{1-x}O_y$ samples

Catalyst	E_a (kJ/mol)	ln$A$
$Fe_{0.05}Ce_{0.95}O_y$	13.1 ± 1.1	4.9 ± 0.2
$Fe_{0.1}Ce_{0.9}O_y$	20.4 ± 3.9	6.2 ± 0.7
$Fe_{0.15}Ce_{0.85}O_y$	8.3 ± 3.2	4.6 ± 0.6
$Fe_{0.2}Ce_{0.8}O_y$	13.4 ± 3.3	4.9 ± 0.6
CeO_2	27.3 ± 9.3	6.9 ± 1.5

listed in Table 4, the order of E_a for different samples is inconsistent with the order of the overall CO oxidation activities. This contradiction is induced by the compensation effect (Bond et al., 2000). The linear correlations between E_a and lnk for different samples are illustrated in Fig. 8. According to the compensation effect, if the relations of the specific activation energies and the pre-exponential factors of a specific reactant for all the types of the catalysts can be fitted into a straight line, the specific reactant will be converted through the similar reaction pathways, replying on the same kind of active centers over different types of catalysts. This means that an increase of the frequency factor (consequent increase of the reaction rate) can be compensated with an increase of the activation energy. Therefore, the order of the overall reaction performances may not always be correlated positively with the absolute

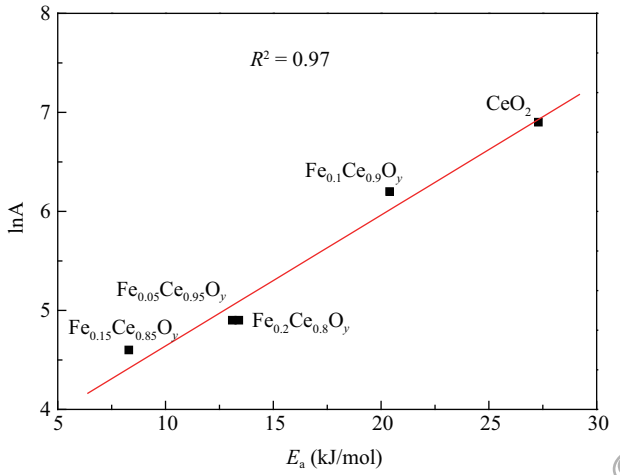

Fig. 8 Compensation effect for CO oxidation of different catalysts.

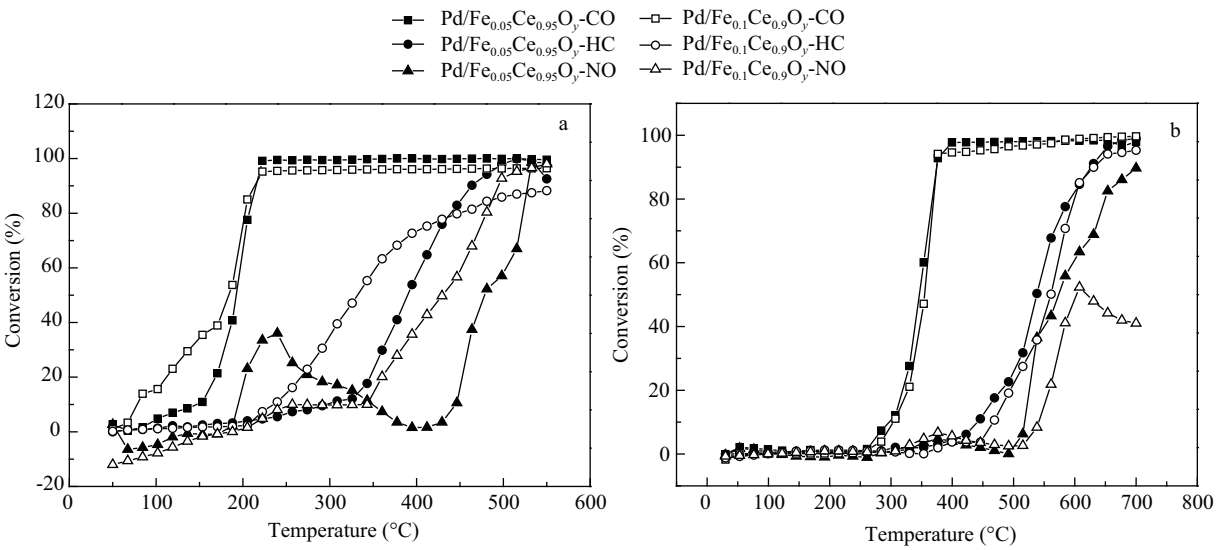

Fig. 9 Catalytic activities of CO, NOx and C_3H_8 of fresh (a) and aged (b) Pd-supported catalysts at simulated outlet exhaust.

values of the apparent activation energies. Such an effect is mainly contributed by the heterogeneity of the surface with multiple active sites. The availability of these active sites not only changes with temperature, but undergoes further modifications induced by the evolutions of reactants and products in gas phases (Botas et al., 2001). As can be seen in Fig. 8, all the points can be fitted in a linear way with limited errors, suggesting the reactions over different types of catalysts investigated share the similar chemical mechanisms. In this work, because the strength of adsorption is weak or the surface coverage by adsorbates is low, the changes of E_a may be mainly caused by different adsorption enthalpies, which cannot reflect the overall catalytic activity (Bond et al., 2000; Botas et al., 2001).

2.4 Three-way catalytic performance

Figure 9 shows the representative stoichiometric light-off behavior of CO, C_3H_8, and NO conversions for all of the samples investigated. CO is oxidized at a much lower temperature than that of C_3H_8. C_3H_8 and NO are converted almost in parallel, indicating the different catalytic process involved in the purification process of automobile exhaust. Temperatures for 50% (T_{50}) and 90% (T_{90}) of exhaust conversion used to evaluate the activity of different catalysts are listed in Table 5. The lower the T_{50} and T_{90}, the higher the activity of catalyst is.

For fresh catalyst, as shown in Fig. 9a, the $Pd/Fe_{0.1}Ce_{0.9}O_y$ sample shows superior three-way activity to $Pd/Fe_{0.05}Ce_{0.95}O_y$. To verify the merit of solid solution in promoting the thermal resistance of catalysts, specific attention was paid to the three-way catalytic performance of aged samples. After hydrothermal aging, all samples showed lower activity for CO, NO_x, and HC conversion due to sintering of precious metal and agglomeration of supports. It is noted that the $Pd/Fe_{0.1}Ce_{0.9}O_y$ sample does not present superiority with respect to $Pd/Fe_{0.05}Ce_{0.95}O_y$. It is considered that the redundant Fe^{n+} species on the surface interact with Pd, which seriously influenced the catalytic activity. It suggested that the solid solution behave superior thermal stability.

Table 5 Temperature required to reach 50% and 90% conversion of catalysts

Catalyst		T_{50} (°C)			T_{90} (°C)		
		CO	HC	NO	CO	HC	NO
$Pd/Fe_{0.05}Ce_{0.95}O_y$	Fresh	193	391	480	212	464	528
	Aged	348	535	568	374	621	–
$Pd/Fe_{0.1}Ce_{0.9}O_y$	Fresh	185	333	383	209	569	502
	Aged	353	561	612	370	635	–

"–": denotes the conversion below 90% under investigated temperature range.

3 Conclusions

$Fe_xCe_{1-x}O_y$ with different Fe/Ce atomic ratio (1–20 mol%) were prepared by sol-gel method. The powder XRD data following Rietveld refinement revealed that the solubility limit of iron oxides in the CeO_2 was 5 mol%. The solid solutions behave superior thermal stability. The three-way catalytic activity results revealed that the redundant iron species separated out of the CeO_2 and interacted with the ceria species on the surface, which seriously influenced the three-way catalytic performance. DOSC results revealed Ce-based materials containing iron oxides with multiple valences contribute to the majority of DOSC. From kinetic analysis, the confirmation of compensation effect revealed that all catalysts share the same mechanism for the separated reactions we investigated.

Acknowledgments

The authors are grateful to the support the National High-Tech Research and Development Program of China (No. 2011AA03A405).

References

Bao H Z, Chen X, Fang J, Jiang Z Q, Huang W X, 2008. Structure-activity relation of Fe_2O_3-CeO_2 composite catalysts in CO oxidation. *Catalysis Letters*, 125(1-2): 160–167.

Bera P, Priolkar K R, Sarode P R, Hegde M S, Emura S, Kumashiro R et al., 2002. Structural investigation of combustion synthesized Cu/CeO_2 catalysts by EXAFS and other physical techniques: Formation of a $Ce_{1-x}Cu_xO_{2-\delta}$ solid solution. *Chemistry of Materials*, 14(8): 3591–3601.

Bond G C, Keane M A, Kral H, Lercher J A, 2000. Compensation phenomena in heterogeneous catalysis: General principles and a possible explanation. *Catalysis Reviews Science and Engineering*, 42(3): 323–383.

Botas J A, Gutiérrez-Ortiz M A, González-Marcos M P, González-Marcos J A, Blanchard G, González-Velasco J R, 2001. Kinetic considerations of three-way catalysis in automobile exhaust converters. *Applied Catalysis B: Environmental*, 32(4): 243–256.

Fan J, Weng D, Wu X D, Wu X D, Ran R, 2008. Modification of CeO_2-ZrO_2 mixed oxides by coprecipitated/impregnated Sr: Effect on the microstructure and oxygen storage capacity. *Journal of Catalysis*, 258(1): 177–186.

Fernández-García M, Martínez-Arias A, Guerrero-Ruiz A, Conesa J C, Soria J, 2002. Ce-Zr-Ca ternary mixed oxides: structural characteristics and oxygen handling properties. *Journal of Cataylsis*, 211(2): 326–334.

Fornasiero P, Fonda E, Di Monte R, Vlaic G, Kašpar J, Graziani M, 1999. Relationships between structural/textural properties and redox behavior in $Ce_{0.6}Zr_{0.4}O_2$ mixed oxides. *Journal of Catalysis*, 187(1): 177–185.

Hori C E, Brenner A, Simon Ng K Y S, Rahmoeller K M, Belton D, 1999. Studies of the oxygen release reaction in the platinum-ceria-zirconia system. *Catalysis Today*, 50(2): 299–308.

Kim D J, 1989. Lattice parameters, ionic conductivities, and solubility limits in fluorite-structure MO_2 oxide ($M = Hf^{4+}$, Zr^{4+}, Ce^{4+}, Th^{4+}, U^{4+}) solid solutions. *Journal of the American Ceramic Society*, 72(8): 1415–1421.

Lambrou P S, Efstathiou A M, 2006. The effects of Fe on the oxygen storage and release properties of model Pd-Rh/CeO_2-Al_2O_3 three-way catalyst. *Journal of Catalysis*, 240(2): 182–193.

Li G S, Smith R L Jr, Inomata H, 2001. Synthesis of nanoscale $Ce_{1-x}Fe_xO_2$ solid solutions via a low-temperature approach. *Journal of American Chemistry Society*, 123(44): 11091–1192.

Li H N, Zhang L, Dai H X, He H, 2009. Facile synthesis and unique physicochemical properties of three-dimensionally ordered macroporous magnesium oxide, gamma-alumina, and ceria-zirconia solid solutions with crystalline mesoporous walls. *Inorganic Chemistry*, 48(10): 4421–4434.

Liang C H, Ma Z Q, Lin H Y, Ding L, Qiu J S, Frandsen W et al., 2009. Template preparation of nanoscale $Ce_xFe_{1-x}O_2$ solid solutions and their catalytic properties for ethanol steam reforming. *Journal of Materials Chemistry*, 19(10): 1417–1424.

Liu F D, He H, 2010. Structure-activity relationship of iron titanate catalysts in the selective catalytic reduction of NO_x with NH_3. *Journal of Physical Chemistry*, 114(40): 16929–16936.

Liu F D, He H, Zhang C B, Feng Z C, Zheng L R, Xie Y N et al., 2010. Selective catalytic reduction of NO with NH_3 over iron titanate catalyst: Catalytic performance and characterization. *Applied Catalysis B: Environmental*, 96(3-4): 408–420.

Mamontov E, Egami T, Brezny R, Koranne M, Tyagi S, 2000. Lattice defects and oxygen storage capacity of nanocrystalline ceria and ceria-zirconia. *Journal of Physical Chemistry B*, 104(47): 11110–11116.

Murugan B, Ramaswamy A V, Srinivas D, Gopinath C S, Ramaswamy V, 2005. Nature of manganese species in $Ce_{1-x}Mn_xO_{2-\delta}$ solid solutions synthesized by the solution combustion route. *Chemistry of Materials*, 17(15): 3983–3993.

Noronha F B, Durão M C, Batista M S, Appel L G, 2003. The role of Ni on the performance of automotive catalysts: evaluating the ethanol oxidation reaction. *Catalysis Today*, 85(1): 13–21.

Péerez-Alonso F J, Granados M L, Ojeda M, Terreros P, Rojas S, Herranz T et al., 2005. Chemical structures of coprecipitated Fe-Ce nixed oxides. *Chemistry of Materials*, 17(9): 2329–2339.

Shen M Q, Wang J Q, Shang J C, An Y, Wang J, Wang W L, 2009. Modification ceria-zirconia mixed oxides by doping Sr using the reversed microemulsion for improved Pd-only three-way catalytic performance. *Journal of Physical Chemistry*, 113 (4): 1543–1551.

Trovarelli A, 1996. Catalytic properties of ceria and CeO_2-containing materials. *Catalysis Reviews Science and Engineering*, 38(4): 439–520.

Vidal H, Kašpar J, Pijolat M, Colon G, Perrichon V, Fally F, 2001. Redox behavior of CeO_2-ZrO_2 mixed oxides: II. Influence of redox treatments on low surface area catalysts. *Applied Catalysis B: Environmental*, 30(1-2): 75–85.

Wang J Q, Shen M Q, Wang J, Gao J D, Ma J, Liu S X, 2011a. CeO_2-CoO_x mixed oxides: structural characteristics and dynamic storage/release capacity. *Catalysis Today*, 175(1): 65–71.

Wang J Q, Zhan B Y, Shen M Q, Wang J, Wang W L, Ma J et al., 2011b. Effects of Fe-doping of ceria-based materials on their microstructural and dynamic oxygen storage and release properties. *Journal of Sol-Gel Science and Technology*, 58(1): 258–269.

Wang X, Gorte R J, 2003. The effect of Fe and other promoters on the activity of Pd/ceria for the water-gas shift reaction. *Applied Catalysis A: General*, 247(1): 157–162.

Xue L, Zhang C B, He H, Teraoka Y, 2007. Catalytic decomposition of N_2O over CeO_2 promoted Co_3O_4 spinel catalyst. *Applied Catalysis B: Environmental*, 75(3-4): 167–174.

Zhang Z L, Han D, Wei S J, Zhang Y X, 2010. Determination of active site densities and mechanisms for soot combustion with O_2 on Fe-doped CeO_2 mixed oxides. *Journal of Catalysis*, 276(1): 16–23.

Zhao M W, Shen M Q, Wang J, 2007. Effect of surface area and bulk structure on oxygen storage capacity of $Ce_{0.67}Zr_{0.33}O_2$. *Journal of Catalysis*, 248(2): 258–267.

JOURNAL OF ENVIRONMENTAL SCIENCES

Journal of Environmental Sciences (Established in 1989)
Vol. 24 No. 4 2012

Supervised by	Chinese Academy of Sciences	**Published by**	Science Press, Beijing, China
Sponsored by	Research Center for Eco-Environmental		Elsevier Limited, The Netherlands
	Sciences, Chinese Academy of Sciences	**Distributed by**	
Edited by	Editorial Office of Journal of	Domestic	Science Press, 16 Donghuangchenggen
	Environmental Sciences (JES)		North Street, Beijing 100717, China
	P. O. Box 2871, Beijing 100085, China		Local Post Offices through China
	Tel: 86-10-62920553; http://www.jesc.ac.cn	Foreign	Elsevier Limited
	E-mail: jesc@263.net, jesc@rcees.ac.cn		http://www.elsevier.com/locate/jes
Editor-in-chief	Hongxiao Tang	**Printed by**	Beijing Beilin Printing House, 100083, China

CN 11-2629/X **Domestic postcode: 2-580** **Domestic price per issue RMB ¥ 110.00**

ISSN 1001-0742